Stem Cell Reports
Article
ISSCR
OPEN ACCESS

The product of BMP-directed differentiation protocols for human primed pluripotent stem cells is placental trophoblast and not amnion

Arun S. Seetharam,[1,2] Ha T.H. Vu,[2,3] Sehee Choi,[4,5] Teka Khan,[4,6] Megan A. Sheridan,[4,5] Toshihiko Ezashi,[4,6,8] R. Michael Roberts,[4,6,7,*] and Geetu Tuteja[2,3,*]

[1]Department of Ecology, Evolution and Organismal Biology, Iowa State University, Ames, IA, USA
[2]Genetics Development and Cell Biology, Iowa State University, Ames, IA, USA
[3]Bioinformatics and Computational Biology, Iowa State University, Ames, IA, USA
[4]Christopher S Bond Life Sciences Center, University of Missouri, Columbia, MO, USA
[5]Department of Obstetrics and Gynecology, University of Missouri School of Medicine, Columbia, MO, USA
[6]Division of Animal Sciences, Bond Life Sciences Center, University of Missouri, Columbia, MO, USA
[7]Department of Biochemistry, University of Missouri, Columbia, MO, USA
[8]Present address: Colorado Center for Reproductive Medicine, 10290 Ridgegate Circle, Lone Tree, CO 80124, USA
*Correspondence: robertsrm@missouri.edu (R.M.R.), geetu@iastate.edu (G.T.)
https://doi.org/10.1016/j.stemcr.2022.04.014

SUMMARY

The observation that trophoblast (TB) can be generated from primed pluripotent stem cells (PSCs) by exposure to bone morphogenetic protein-4 (BMP4) when FGF2 and ACTIVIN signaling is minimized has recently been challenged with the suggestion that the procedure instead produces amnion. Here, by analyzing transcriptome data from multiple sources, including bulk and single-cell data, we show that the BMP4 procedure generates bona fide TB with similarities to both placental villous TB and TB generated from TB stem cells. The analyses also suggest that the transcriptomic signatures between embryonic amnion and different forms of TB have commonalities. Our data provide justification for the continued use of TB derived from PSCs as a model for investigating placental development.

INTRODUCTION

For a variety of ethical and practical reasons, there is considerable interest in creating *in vitro* model systems that mimic the early stages of human placental development (Zhou et al., 2021). Ever since Xu et al. (2002) demonstrated that when human embryonic stem cell (hESC) lines, with what we now know to be primed/epiblast-type features, are exposed to bone morphogenetic protein-4 (BMP4) they express an extensive range of markers characteristic of trophoblast (TB), numerous investigators have chosen to refine this model to study the early origins of placental TB (Horii et al., 2016, 2020; Roberts et al., 2018). Although the protocols for achieving TB differentiation by BMP4 priming have differed in detail, most strictly exclude factors used to maintain hESC pluripotency, specifically fibroblast growth factor (FGF2) and members of the transforming growth factor β (TGF-β) family, which includes NODAL and ACTIVIN-A. However, simply omitting these factors from the culture medium may not be sufficient to suppress their autocrine effects (Ezashi et al., 2012; James et al., 2005). For this reason, improved differentiation can be achieved by the addition of ACTIVIN-A/NODAL/TGF-β signaling inhibitor (A83-01) and FGF2 signaling inhibitor (PD173074), in addition to BMP4 (so-called BAP conditions). Upon exposure to BAP, almost all cells become transiently positive for CDX2 at 24–48 h and upregulate the pan-TB marker KRT7 (Amita et al., 2013; Yabe et al., 2016; Yang et al., 2015). These colonies contain HLA-G-positive cells by day 3–4, which reach a maximum by day 6 and then decline (Yang et al., 2015) and begin to form syncytialized areas by day 5–6, such that both syncytialized and HLA-G-positive subpopulations can be readily isolated and analyzed (Telugu et al., 2013; Yabe et al., 2016; Yang et al., 2015). As an alternative to the BAP protocol, BMP4 treatment can be performed in a minimal stem cell medium containing an inhibitor (IWP-2) of WNT to yield a relatively undifferentiated cytotrophoblast (CT) population, which can then be directed toward either CGB-positive syncytiotrophoblast (STB) or HLA-G-positive extravillous TB (EVT)-like cells (Horii et al., 2016). Recently, the concept that it is possible to generate CT and more advanced lineages, such as STB, from human epiblast/primed ESCs and induced pluripotent stem cells (iPSCs) by using BMP4, especially as it relates to the BAP model and that described by Horii et al. (2019), has been challenged (Guo et al., 2021; Io et al., 2021). It has instead been suggested that the resulting cells more resemble developing human amnion than they do TB. Here, by analyzing transcriptome data from multiple sources (Table S1), we present evidence clearly showing that the standard BAP protocol generates bona fide TB with close similarity to that of differentiated TB stem cells (TSCs) and TB present in early-first-trimester human placentas.

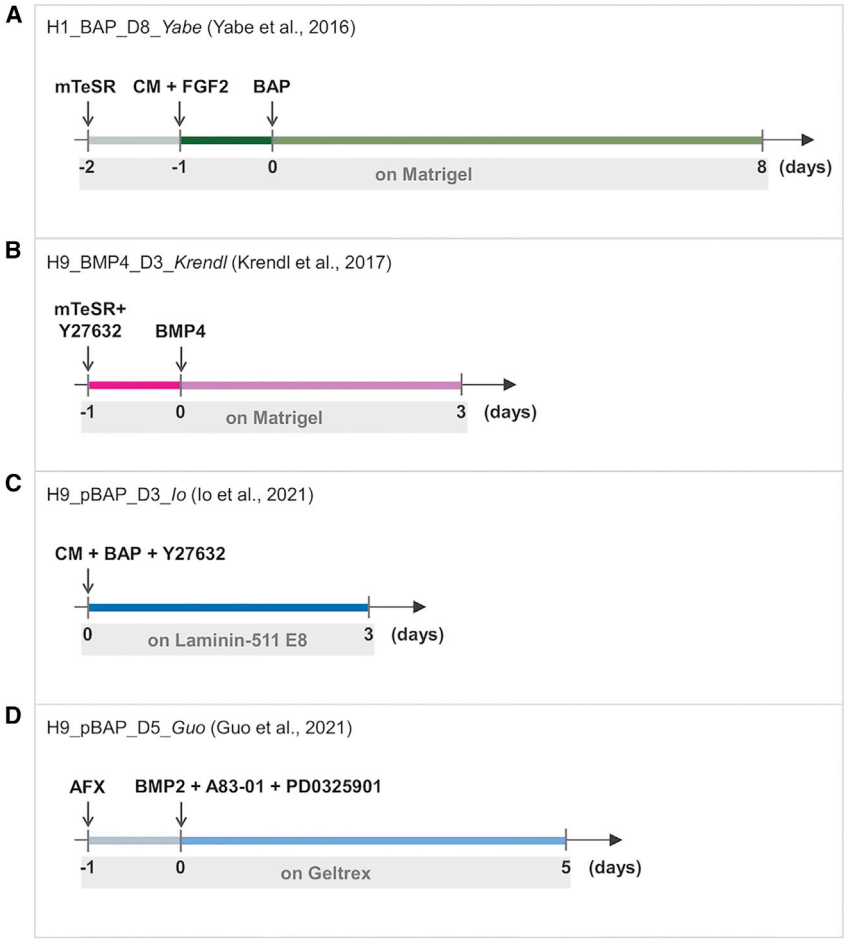

Figure 1. Comparison of procedures for BMP4 or BAP treatment among Yabe et al., Krendl et al., Io et al., and Guo et al.

(A) For the generation of BAP_D8_*Yabe* (Yabe et al., 2016), primed H1 ESCs were seeded on a Matrigel-coated plate and cultured with mTeSR1. On the day following passaging, the medium was replaced with hESC medium (DMEM/F12 containing 20% KSR, 1 mM L-glutamine, 0.1 mM 2-ME, 1% NEAA), which had been conditioned by irradiated mouse embryonic fibroblasts (iMEFs), called MEF-conditioned medium (CM), and supplemented with 4 ng/mL FGF2. After an additional day, the medium was changed to hESC medium containing 10 ng/mL BMP4, 1 μM A83-01, and 0.1 μM PD173074 (BAP) for 8 days.

(B) For the generation of BMP4_D3_*Krendl* (Krendl et al., 2017), primed H9 ESCs were dissociated using Accutase and seeded as single-cell monolayers on Matrigel-coated plate and cultured with mTeSR1 medium supplemented with 10 μM Y-27632. After 16–18 h, the medium was changed to RPMI1640, containing Glutamax and B27 without insulin, and supplemented with 50 ng/mL BMP4 for 72 h.

(C) For the generation of pBAP_D3_*Io* (Io et al., 2021), primed H9 ESCs were dissociated into single cells with trypsin/EDTA and seeded on a Laminin-511 E8-coated plate and cultured with MEF-CM supplemented with BAP and 10 μM Y27632 for 3 days.

(D) For the differentiation of primed hPSCs in Guo et al. (Guo et al., 2021), primed H9 ESCs were seeded on Geltrex-coated plate and cultured with AFX medium, which contains N2B27 basal medium with 5 ng/mL Activin A, 5 ng/mL FGF2, and 2 μM XAV. The next day, the medium was replaced with N2B27 basal supplemented with 50 ng/mL BMP2, 1 μM A83-01, and 1 μM PD0325901 for 5 days. In this study, RNA-seq data generated from H1_BAP_D8_*Yabe*, H9_BMP4_D3_*Krendl*, and H9_pBAP_D3_*Io* were used for the comparative analyses among primed ESC-derived TB models by different protocols. There is no available RNA-seq data for H9_pBAP_D5_*Guo*.

RESULTS

RNA sequencing (RNA-seq) analyses of three BMP4-based protocols used for PSC differentiation

One possible reason that different conclusions have been reached about the identity of cells resulting from BMP4 or BAP differentiation is because of variations in the methods used by different investigators (Figure 1). To understand whether or not the different protocols are driving differentiation of primed-type human PSCs toward TB, and to determine what specific kind of TB appears to be formed, we compared transcriptomes of differentiated and undifferentiated cells from the three protocols for which RNA-seq data had previously been generated (Figure 1). Io et al. used primed H9 hESCs and a modified BAP treatment for 3 days (H9_pBAP_D3_*Io*) (Io et al., 2021). Krendl et al. also used BMP4 treatment (at 50 rather than 10 ng/mL) but without inhibitors for 3 days (H9_BMP4_D3_*Krendl*) (Krendl et al., 2017). This higher level of BMP4 might be expected to provide an accelerated rate of TB differentiation than providing 10 ng/mL (Xu et al., 2002). In contrast, Yabe et al. employed the standard BAP protocol (Amita et al., 2013) with an extended time period (8 days), when an extensive number of markers associated with STB had emerged (Yabe et al., 2016). These cells (H1_BAP_D8_>70_*Yabe*) are BAP-differentiated cells that had been collected on a 70 μm filter immediately after harvesting. A subsequent filtration step removed cells >40 μm, with the final filtrate providing a population of predominantly mononucleated cells <40 μm in diameter (H1_BAP_D8_<40_*Yabe*).

As expected, there are many genes differentially expressed when comparing undifferentiated and differentiated cells within each treatment protocol (Data S1; Figure 2). To determine how genes upregulated in each cell

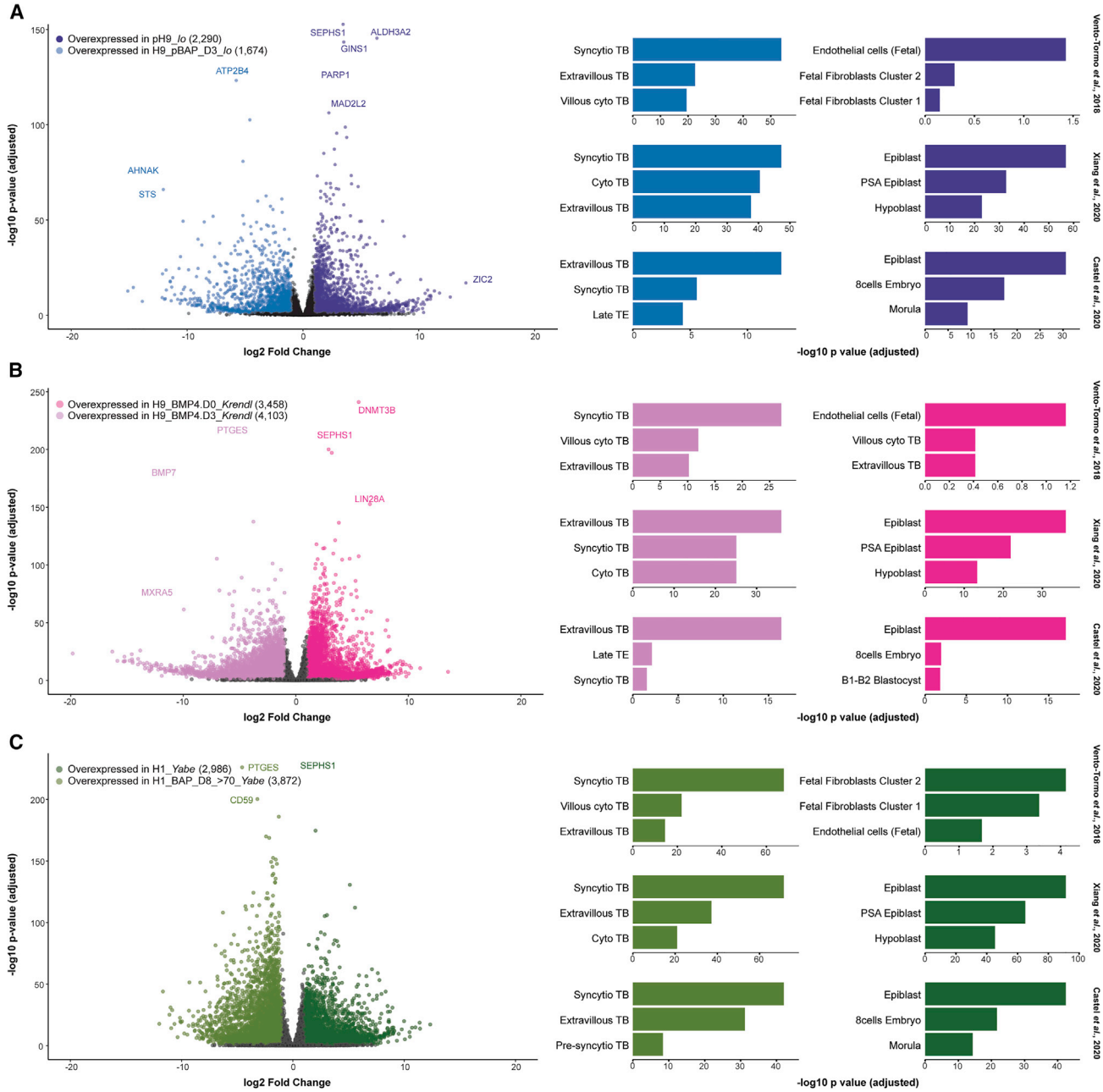

Figure 2. Upregulated genes and cell enrichment analyses of undifferentiated and differentiated datasets

(A–C) The datasets were obtained by using BMP4-based protocols of (A) *Io* (pH9 versus H9_pBAP_D3), (B) *Krendl* (H9_BMP4 versus H9_BMP4_D3), and (C) *Yabe* (H1_Yabe versus H1_BAP_D8_>70).

In the volcano plot, the darker shade is undifferentiated, showing upregulated genes of pH9 (purple), H9_BMP4 (darker pink), and H1_Yabe (darker green). The lighter shade is their differentiated counterpart, H9_pBAP_D3 (lighter blue), H9_BMP4_D3 (lighter pink), and H1_BAP_D8_>70 (lighter green). Only genes with $|\log2\text{fold}| \geq 1$ and adjusted p value (padj) ≤ 0.05 are colored. The cell enrichment results of the upregulated genes are depicted as bar plots (color coordinated), with the top chart using the Vento-Tormo et al. (2018) dataset for enrichment analyses, the middle using the Xiang et al. (2020) dataset, and the bottom using the combined Zhou et al. (2019) and Petropoulos et al. (2016) datasets (curated by Castel et al., 2020). Only the three most-enriched fetal cell types are shown here (see Figure S1 for the full cell enrichment results).

type are related to cells of the first-trimester placenta, we used the PlacentaCellEnrich program (Jain and Tuteja, 2021), which determines if a given set of input genes (for example, genes upregulated in undifferentiated or differentiated cells) are enriched for genes with cell-type-specific expression in first-trimester human placenta (Vento-Tormo et al., 2018). In the PlacentaCellEnrich program, cell-type-specific expression is defined by using an algorithm from the Human Protein Atlas (Uhlén et al., 2015). The definition includes not only genes that are more highly expressed in one cell type compared with each other cell type but also genes that have higher expression in 2–7 cell types compared with the remaining cell types. Therefore, when using this algorithm, a gene that is STB specific could simultaneously be considered EVT specific. For all three differentiation protocols, genes upregulated in the BMP4-exposed cells are enriched (defined as $-\log_{10}$(adjusted p value $\geq$ 1.3)) for transcripts with STB-specific expression (Figures 2 and S1). By contrast, genes upregulated in undifferentiated cells are not enriched for any TB-specific markers (Figures 2 and S1).

However, comparisons of the BMP4-exposed cells with first-trimester-placenta gene sets do not provide information as to how these cells might resemble cells present during early-embryo differentiation when a peripheral mass of invasive STB first emerges as the embryo implants. Therefore, we also made custom gene sets to perform cell-type enrichment analysis with single-cell (sc) RNA-seq data from a blastocyst culture system (Xiang et al., 2020) and human embryo cultures, namely from Zhou et al. (2019), who used embryos at days 6, 8, 10, 12, and 14, and Petropoulos et al. (2016), who examined cleavage-stage embryos and day 5–7 blastocysts. The scRNA-seq information from Zhou et al. (2019) and Petropolous et al. (2016) had been integrated previously by Castel et al. (2020) and is herein referred to as Zhou/Petro embryo data (Castel et al., 2020; Petropoulos et al., 2016; Zhou et al., 2019). Using cell-type-specific enrichment analysis with cell types present in the early embryo, we again observe that genes upregulated in H9_pBAP_D3_*Io*, H9_BMP4_D3_*Krendl*, and H1_BAP_D8_>70_*Yabe* are enriched for TB-specific gene expression, whereas, in this new comparison, genes upregulated in the undifferentiated cells are all enriched for epiblast markers (Figures 2 and S1). Genes upregulated in H9_pBAP_D3_*Io* and H9_BMP4_D3_*Krendl* are more enriched for EVT-specific gene expression than for STB-specific gene expression (enrichment values as $-\log_{10}$(adjusted p value) for EVT and STB are 12.95 and 5.57 in H9_pBAP_D3_*Io* with the Castel et al. dataset and 16.40 and 1.53 in H9_BMP4_D3_*Krendl* with the Castel et al. dataset, respectively), whereas genes upregulated in H1_BAP_D8_>70_*Yabe* are more biased toward STB ($-\log_{10}$(adjusted p value) for EVT and STB are 31.16, and 41.99, respectively).

Comparison of genes upregulated between the BMP4-based protocols

To gain further insights into the results from the previous section, we next compared expression profiles of the differentiated cells derived from the aforementioned protocols. Many differentially expressed genes distinguished the three groups (Data S1; Figure 3). We again use cell-type-specific enrichment analysis with both first-trimester-placenta cell data (Vento-Tormo et al., 2018) and early-embryo data (Xiang et al., 2020 and Castel et al., 2020, i.e., Zhou/Petro data). Genes upregulated in H1_BAP_D8_>70_*Yabe* generally have cell-type-specific expression for STB when compared with both H9_BMP4_D3_*Krendl* and H9_pBAP_D3_*Io* (Figures 3 and S2). Genes upregulated in H9_BMP4_D3_*Krendl* have cell-type-specific expression for EVT when compared with H1_BAP_D8_>70_*Yabe* and for both EVT and STB when compared with H9_pBAP_D3_*Io* (Figures 3 and S2). By contrast, H9_pBAP_D3_*Io* does not have significant enrichment (defined as $-\log_{10}$(adjusted p value $\geq$ 1.3)) for any TB lineage when using the first-trimester-placenta data but demonstrate a significant enrichment for epiblast-specific expression when used with the Xiang and Zhou/Petro embryo data (Figures 3 and S2). Cells that are less differentiated tend to have enrichment of epiblast-specific expression, as we observed when analyzing genes upregulated in undifferentiated ESCs.

Because the differentiation protocol used in Yabe et al. results in cells of different sizes, including small mononucleated cells and variably sized regions of syncytium, we also compared H9_pBAP_D3_*Io* and H9_BMP4_D3_*Krendl* with BAP-differentiated H1 cells that had passed through a 40 μm filter (H1_BAP_D8_<40_*Yabe*) (Yabe et al., 2016). From cell-type-specific expression analysis, we observe that while genes upregulated in H1_BAP_D8_<40_*Yabe* are enriched for STB-specific expression compared with H9_pBAP_D3_*Io*, genes upregulated in H9_BMP4_D3_*Krendl* are enriched for STB-specific expression compared with H1_BAP_D8_<40_*Yabe* (Figure S3). Together, these results indicate that, of the three differentiation protocols analyzed, H9_pBAP_D3_*Io* provides a population of cells least differentiated toward STB. Next in the progression toward differentiated STB are, respectively, H1_BAP_D8_<40_*Yabe* and H9_BMP4_D3_*Krendl*. Finally, H1_BAP_D8_>70_*Yabe* appear to represent the most robust differentiation to STB.

Principal-component analysis (PCA) of expression profiles from stem cells, various forms of *in vitro* and *in vivo* differentiated TB, and amnion

We next used PCA to compare gene expression profiles of several cell types, including undifferentiated hESCs, TSCs, trophectoderm (TE), CT, STB, EVT differentiated *in vitro*

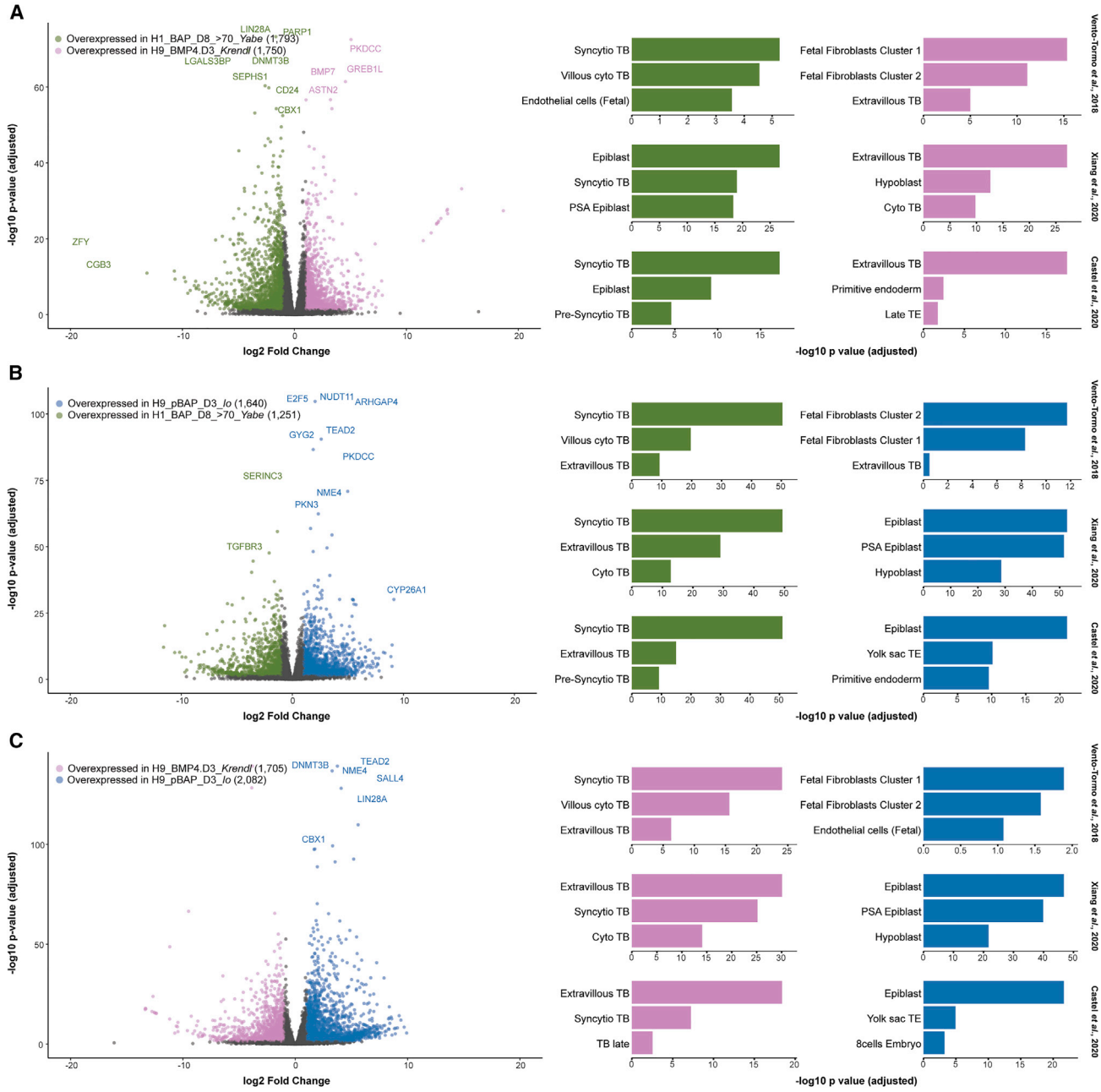

Figure 3. Upregulated genes and cell enrichment analyses of differentiated cells from BMP4-based protocols of Io et al., Krendl et al., and Yabe et al.

(A–C) The comparisons include (A) H9_BMP4_D3 (light pink) versus H1_BAP_D8_>70 (light green), (B) H1_BAP_D8_>70 (light green) versus H9_pBAP_D3 (light blue), and (C) H9_pBAP_D3 (light blue) versus H9_BMP4_D3 (light pink). In the volcano plots, only genes with $|\log2fold| \geq 1$ and $padj \leq 0.05$ are colored. The cell enrichment results of the upregulated genes are depicted as bar plots (color co-ordinated), with the top chart using the Vento-Tormo et al. (2018) dataset for enrichment analyses, the middle using the Xiang et al. (2020) dataset, and bottom using the combined Zhou et al. (2019), and Petropoulos et al. (2016) datasets (curated by Castel et al., 2020). Only the three most-enriched fetal cell types are shown here (see Figure S2 for the full cell enrichment results and Figure S3 for enrichment results that include H1_BAP_D8_<40).

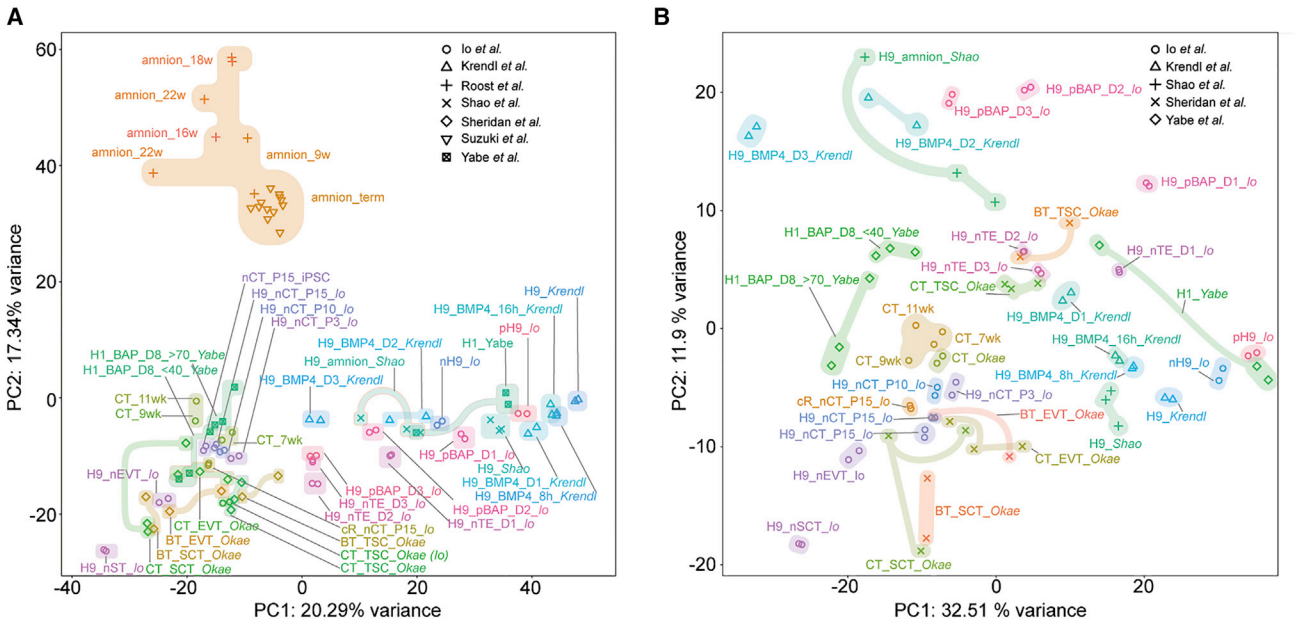

Figure 4. Principal-component analysis (PCA) plots

(A) PCA plot showing the clustering of various datasets used in this study.

(B) PCA plot showing the clustering of datasets (without fully differentiated amnion sets) used in this study. Each color represents the treatment (cell type and/or media/growth condition), and the shape represents the study from which the samples were derived (see Table S1 for more details). PCA plots for additional components and variance explained by each component (scree plots) are shown in Figure S4.

from various sources, and BAP-treated cells (Figure 4A) (Io et al., 2021; Krendl et al., 2017; Sheridan et al., 2021; Yabe et al., 2016). Our analysis also included TB isolated from placental villi and amnion cells derived either from hESCs or isolated at different stages of gestation (Io et al., 2021; Roost et al., 2015; Shao et al., 2017; Suzuki et al., 2016). For a full list of datasets and abbreviations, see Table S1.

Visualization of different PCs (Figures 4A and S4A–S4C) as well as an examination of Euclidean-distance calculations between samples using PCA projection coordinates (PC 1–3) (Table S2) leads to four main observations. First, while amnion cells obtained from 9 weeks of gestation through term are not identical across gestation, they generally cluster away from other cell types, including the cells reported to be amnion and derived from hESCs (H9_amnion_*Shao*) (Shao et al., 2017) (Figure 4A). Second, H1_BAP_D8_>70_*Yabe* and H1_BAP_D8_<40_*Yabe* cluster more closely with differentiated TB derived from a variety of sources, including first-trimester placental villi (CT_7wk, CT_9wk, CT_11wk), than with amnion samples obtained during pregnancy (Figures 4A and S4; Table S2). Third, the pluripotent H1 and H9 cells, e.g., H9_*Krendl*, pH9_*Io*, and H1_*Yabe*, and the 8 and 16 h *Krendl* cells cluster quite closely, but, by day 2 of BMP4 exposure, there has been a clear shift of the H9_BMP4_D2_*Krendl* and H9_pBAP_D2_*Io* cells away from the general neighborhood of the pluripotent cells and toward TB cells (Figure 4A; Table S2). Finally, for BAP-treated cells, as well as CT and other TB, we generally observe more similarity to the *Shao* dataset of presumed embryonic amnion (H9_amnion_*Shao*) than amnion obtained during pregnancy (Figures 4A, S4B, and S4C; Table S2).

To investigate additional differences between H9_pBAP_D3_*Io*, H9_BMP4_D3_*Krendl*, and H1_BAP_D8_>70_*Yabe* and how these differentiated cells relate to other placenta cell types, we again have used PCA but excluded the amnion samples obtained during pregnancy. We focused on the first three principal components, which account for 53.47% of the variance (Figure S4D), plotted each pairwise plot for PC1, PC2, and PC3 (Figures 4B, S4E, and S4F), and again calculated Euclidean distances between samples using the PCA projection coordinates (Table S3). We note that in this assembly, PC1 accounts for the highest variance (32.51%). From these new plots, the observations made above from the PC1 versus PC2 pairwise plot shown in Figure 4A and Euclidean distances in Table S2 are generally confirmed. For example, H1_BAP_D8_>70_*Yabe* data again cluster closely with specific TB cell types: either CT from first-trimester placentas (PC1 versus PC2 and PC2 versus

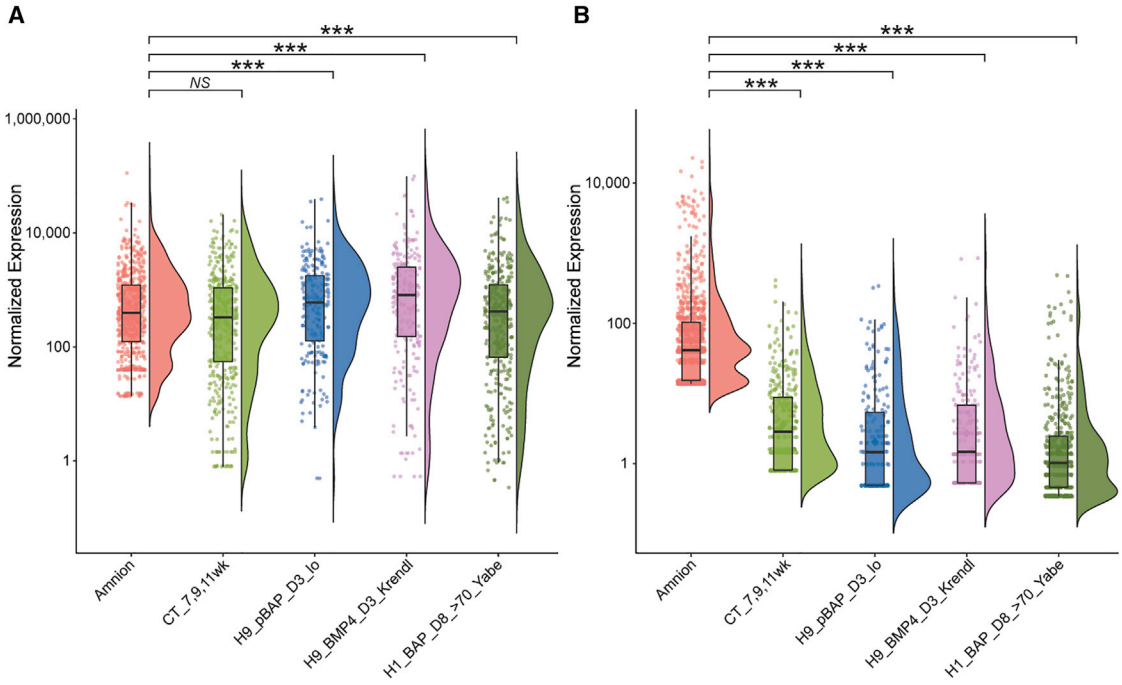

Figure 5. Comparing expression of selected genes in various datasets

(A) Violin-box plot showing the expression of genes upregulated in 9 week amnion samples compared with the 9 week placenta (gene list obtained from Figure 6B of *Io* et al.), in H9_pBAP_D3, H9_BMP4_D3, and H1_BAP_D8_>70 samples.

(B) Violin plot showing the expression of amnion marker genes identified using TissueEnrich (fold change >10) from all amnion datasets available in Roost et al. for the same datasets in (A). The expression differences were compared using the non-parametric Dunn's (Dunn, 1964) test of multiple comparisons following a significant Kruskal-Wallis test (Kruskal and Wallis, 1952), with p values adjusted with the Benjamini-Hochberg method (highly significant, ***p < 0.001; non-significant, *NS*). For (A), associated padj values for amnion versus CT, amnion-H9_pBAP_D3, amnion-H9_BMP4_D3, and amnion-H1_BAP_D8_>70 are 0.11×10^{-1}, 9.78×10^{-9}, 4.34×10^{-13}, and 1.61×10^{-4}, respectively. Similarly, for (B), padj values for amnion versus CT, amnion-H9_pBAP_D3, amnion-H9_BMP4_D3, and amnion-H1_BAP_D8_>70 are 6.82×10^{-69}, 3.16×10^{-37}, 2.39×10^{-31}, and 5.41×10^{-20}, respectively.

See also Figure S5.

PC3) (Figures 4B and S4F) or STB (PC1 versus PC3) (Figure S4E). H9_pBAP_D3_*Io* data, on the other hand, tend to cluster further away from differentiated TB and nearer to H9_BMP4_D2_*Krendl* (PC1 versus PC2 and PC2 versus PC3) (Figures 4B and S4F; Table S3), although both these datasets also have some similarity to CT and EVT (Figure S4E; Table S3). The data presented in the PCA plots are largely in agreement with the analysis presented earlier (Figure 2), namely that H9_pBAP_D1-3_*Io* are on a similar but somewhat delayed course toward TB, relative to the cells of Krendl et al. (2017), while H1_BAP_D8_>70_*Yabe* appear to be fully differentiated TB.

The gene signature of amnion and the relationship to TB

We then investigated genes described as having high expression in amnion tissues (Roost et al., 2015) more carefully and examined their expression in TB. In this regard, we focused our attention on the dataset that appeared to have the most differentiated TB, i.e., H1_BAP_D8_>70_*Yabe*, and the datasets that might have less differentiated TB, namely H9_pBAP_D3_*Io* and H9_BMP4_D3_*Krendl*. We also included datasets from first-trimester CT (weeks 7, 9, and 11 from Io et al., 2021) in the analysis to represent cells that are definitively TB. Overall, these data were not particularly informative. For example, we found that when comparing normalized expression counts for genes that were previously identified as upregulated in 9 week amnion (relative to 9 week placenta; data from Figure 6B of Io et al., 2021), H9_BMP4_D3_*Krendl* had higher overall expression of the amnion-upregulated genes than any of the other datasets, including amnion itself (Figures 5A and S5A; Table S4) (average normalized expression of previously defined amnion genes: 1,164.81 in amnion, 1,067.5 in CT, 1,706.64 in H9_pBAP_D3_*Io*, 3,162.65 in H9_BMP4_D3_*Krendl*, and 1,606.21 in H1_BAP_D8_>70_*Yabe*). Further, the Spearman correlation between the two replicates of 9 week amnion is only

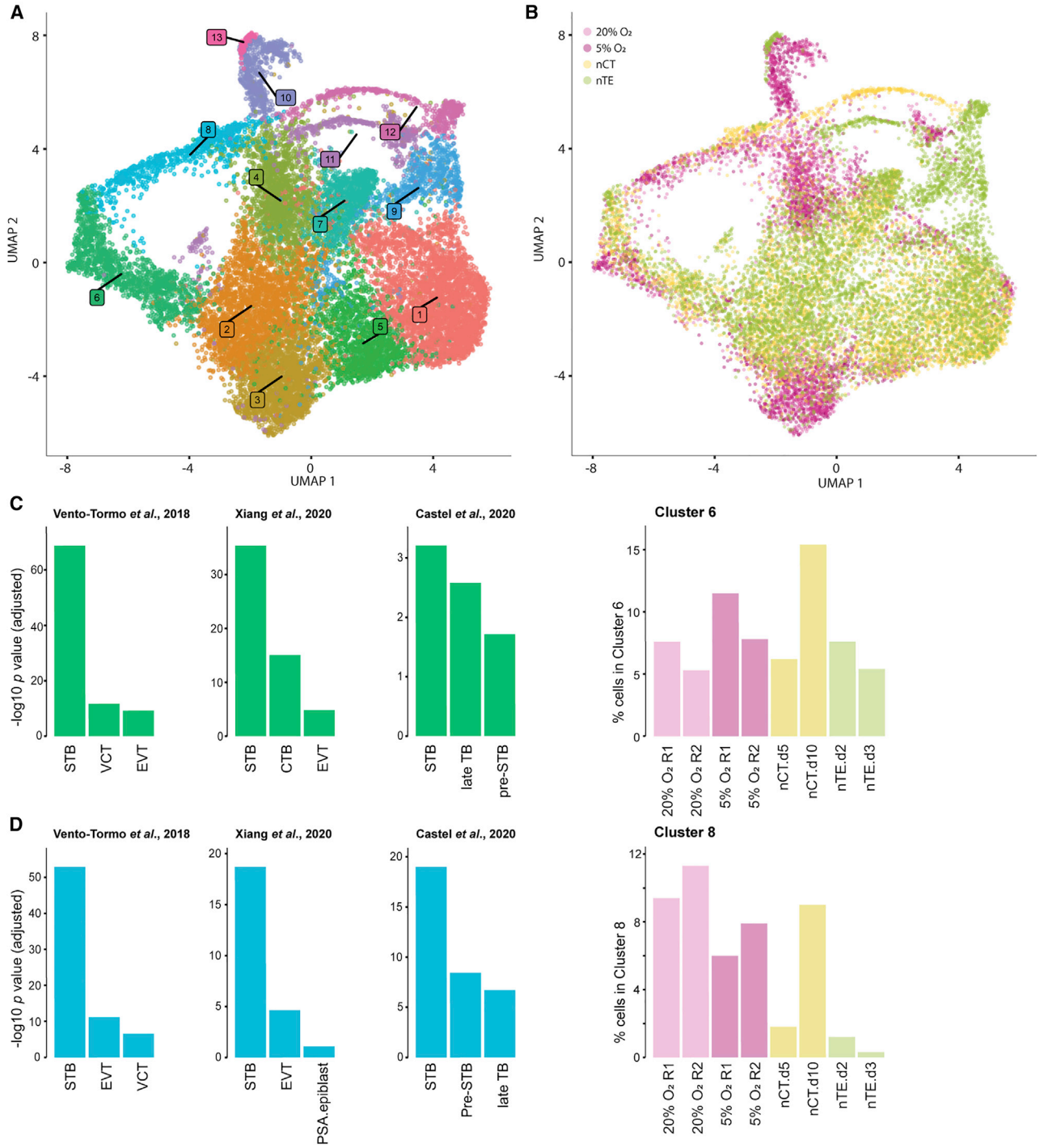

Figure 6. Visualization of clusters generated from single-nucleus and single-cell RNA sequencing analyses

(A) Visualization of clusters generated from single-cell and single-nucleus data colored according to assignment by clustering analysis. (B) Nuclei/cells visualized according to cell type and growth conditions. H1_BAP_D8_20pcO2_*Khan* (pink), H1_BAP_D8_5pcO2_*Khan* (purple), nCT (H9_nCT_D5_*Io* and H9_nCT_D10_*Io*) (yellow), and nTE (H9_nTE_D2_*Io* and H9_sc.nTE_D3_*Io*) (green) are shown. Each dot represents a nucleus/cell.

(legend continued on next page)

slightly higher than the correlation between 9 week amnion and 9 week CT (see correlation values in Figure S5B), indicating similarity of overall expression profiles between 9 week amnion and 9 week CT. Additionally, these amnion-upregulated genes have similar levels of expression in cells differentiated by the Okae protocol as they do in amnion itself (Figure S5C, no significant difference between expression distributions). Based on these results, we sought to identify a more-specific list of amnion marker genes.

To this end, we used the TissueEnrich framework to create a list of 292 amnion-expressed genes that are not well represented in TB cells derived by the Okae protocol (Figure S5D). In contrast to the genes shown in Figure 5A, the TissueEnrich-based amnion gene list results in major differences in gene expression between amnion and TB datasets, including first-trimester CT (Figures 5B, S5E, and S5F). We do note that there is high variability in expression of these genes in amnion samples across gestation (Figures S5E and S5F). Only seven of the genes (*ACMSD*, *AQP9*, *CLDN22*, *TMEM174*, *MCCD1*, *SOX11*, and *HBA1*) have high expression ($\geq$100) across all amnion samples, two of which (*MCCD1* and *TMEM174*) have very high expression ($\geq$3,000) across all samples of fetal-derived amnion (Table S5). Importantly, however, we observe significantly lower expression of the TissueEnrich-derived potential amnion markers in H1_BAP_D8_>70_*Yabe*, H9_pBAP_D3_*Io*, and CT (Figures 5B, S5E, and S5F; Table S5).

Analysis of cell populations in BAP-treated, naive PSC-derived CT-like (nCT), and naive PSC-derived TE-like (nTE) cells

We recently carried out single-nuclei (sn) RNA-seq on BAP-treated cells differentiated under 5% and 20% O_2 conditions in an attempt to address the heterogeneity of cell populations that comprise the colonies at day 8 of BAP treatment, as well as the effects of O_2 on differentiation (Khan et al., 2021). The BAP-differentiated colonies provided at least nine clusters of nuclei, all enriched for TB markers (Khan et al., 2021). To determine whether these clusters correspond to those found in other TB datasets, we integrated the Khan et al. BAP snRNA-seq data with the nCT and nTE scRNA-seq data of Io et al. (Figures 6A and 6B). We observe many clusters, including 5, 6, 7, 8, and 11, that share nuclei from the BAP-differentiated colonies (including those differentiated under both 5% and 20% O_2), nCT, and/or nTE (Figures 6B and S6). Of these, two (cluster 6 and 8) are highly enriched for genes with STB-specific expression (Figures 6C and 6D) and are discussed further below. Relative to the total number of nuclei/cells in the sample, clusters 4 and 10 have more than a 5-fold higher percentage of BAP-differentiated nuclei than either nTE or nCT cells and show some enrichment for EVT-specific gene expression (Figure S6). Cluster 9, on the other hand, is contributed uniquely by nTE and enriched for early TE-specific genes (Figure S6). Cluster 12 is shared by nTE (mainly left subcluster) and nCT (mainly right subcluster) but not BAP nuclei (Figure 6B) and demonstrates an epiblast signature (Figure S6). Clusters 1 and 2 contain more than a 3-fold higher percentage of nCT and nTE cells than BAP-differentiated nuclei and were enriched for CT-specific gene expression (Figures 6B and S6). Other clusters, like 3, 5, 7, and 11, which have higher proportions of either BAP-differentiated cells, nCT, or nTE, are difficult to classify (Figures 6B and S6). The clusters with nuclei unique to BAP-differentiated cells could represent different kinds of CT, based on the expression of general TB markers (Khan et al., 2021) but lack of EVT and STB-specific signatures.

As discussed above, we were able to identify two distinct populations of cells with STB identity (clusters 6 and 8) (Figures 6C, 6D, and S6). While cluster 6 contained cells/nuclei from nCT, nTE, and differentiated BAP colonies, cluster 8 largely lacked representation from nTE cells. Based on the datasets generated by Xiang et al. (2020) from 3D-cultured human pre-gastrulation embryos, cluster 6 has marker genes enriched for both STB- and CT-specific expression (enrichment values as -$\log_{10}$(adjusted p value) for STB and CT: 35.37 and 15.04, respectively), while cluster 8 has enrichment for STB-specific expression but lacks CT-specific expression (Figures 6C and 6D) (enrichment values as -$\log_{10}$(adjusted p value) for STB and CT: 18.70 and 1.30, respectively). Similarly, from the Zhou/Petro combined dataset of early embryos (Castel et al., 2020; Petropoulos et al., 2016; Zhou et al., 2021), we observe clusters 6 and 8 to be enriched for genes with STB-specific expression, although cluster 6 has higher significance for late-TB-specific genes rather than pre-STB-specific genes (Figure 6C), while cluster 8 has higher significance for pre-STB-specific genes than late-TB-specific genes (Figure 6D). Based on these observations, there seem to be two possibilities: either clusters 6 and 8 really do represent cells from early- and late-stage STB, respectively, or there are two lineages of STB, as has been suggested previously

(C and D) The cell enrichment bar plots for the marker genes of clusters 6 and 8 (genes with |fold change| $\geq$ 1.5 and padj $\leq$ 0.05) along with the composition of nuclei/cells for different treatments (as percentages, relative to the total number of nuclei/cells in the condition) (see Figure S6 for cell composition of other clusters). The cell enrichment results were done using the Vento-Tormo et al. dataset, the Xiang et al. dataset, and the combined Zhou et al. and Petropoulos et al. datasets (curated by Castel et al.). Only the three most-enriched fetal cell types are shown here (see Figure S6 for the full cell enrichment results).

for mature placenta (Tsang et al., 2017). Perhaps most importantly, the information from Figure 6 confirms that many, but not all, clusters from the snRNA-seq analyses of BAP-differentiated H1 primed-type cells align with ones from the scRNA-seq analyses of TB differentiated *in vitro* from naive state ESCs. These similarities include the presence of two kinds of STB.

DISCUSSION

The experiments of Io et al. (2021) and Guo et al. (2021) showed that human naive PSCs can be converted directly to cells with a TE phenotype and then maintained in a self-renewing stem cell state resembling that described by Okae et al. (2018) for TSCs generated directly from human blastocysts and first-trimester villous placental tissue. When given appropriate stimuli, both varieties of TSCs can progress through CT intermediaries to differentiate into EVT and STB, thereby recapitulating the trajectory from pre- to post-implantation stages of early pregnancy. As no similar progression has been achieved with mouse naive PSCs, Guo et al. attribute the ability of human naive PSCs to convert to TB to their regulative flexibility compared with the mouse (Guo et al., 2021). They speculate, however, that no such plasticity and capacity to revert to the TB lineage exists with primed human PSCs, arguing that, once the human epiblast reaches the post-implantation stage of development, that opportunity has been lost. Instead, both Io et al. and Guo et al. contend that the protocols that use BMP4 to create TB from primed PSCs, in fact, produce amnion, which represents the first lineage to separate from the embryonic disc subsequent to segregation of hypoblast and epiblast.

We examine this latter assertion in detail here and arrive at different conclusions. Io et al. based their arguments largely on inferences drawn from a transcriptome dataset they generated by exposing primed PSCs to BAP conditions but following a protocol somewhat different from those used by others practicing the technology (Amita et al., 2013; Roberts et al., 2018; Yabe et al., 2016) (Figure 1). In particular, Io et al. stopped their experiments not at day 8 but at day 3, which sits in a transition where there is upregulation of several transcription factors and other gene products linked to the emergence of TB but also at a time preceding the appearance of most markers of mature TB lineages and before the complete downregulation of genes associated with pluripotency (Krendl et al., 2017; Marchand et al., 2011; Schulz et al., 2008). It is not surprising, therefore, that the transcriptomes generated by Io et al. (2021) at day 3 of differentiation differ markedly from those published by others, including Yabe et al. (2016), at later stages of differentiation (Figure 3). The same conclusion that the BAP-differentiated cells are amnion was made by Guo et al. (2021), who employed a 5 day differentiation period in the presence of BMP2, rather than BMP4, and the MEK inhibitor PD0325901, instead of the FGF2 signaling inhibitor PD173074, to drive the process (Figure 1).

Whether BMP2 is equipotent to BMP4 on PSC differentiation is unclear, as Xu et al. used much higher concentrations of BMP2 than BMP4 in their experiments and did not make direct comparisons (Xu et al., 2002). BMP4 and BMP2 share 80% identity in their amino-acid sequence, and so it is not implausible that both would have similar biological effects on target cells. However, based on studies in other systems where BMP2 and BMP4 have been compared for biopotency, they do not behave identically (Gao et al., 2013; Shu et al., 2011; Yang et al., 2019). It is possible that, at the same concentration (10 ng/mL), differentiation to TB in response to BMP2 may be slower than with BMP4. Therefore, the use of an optimized BAP protocol is recommended if the desired cell type is that of a differentiated TB.

From our analysis, it is clear that the cells generated by the standard BAP protocol and present at day 8 of differentiation are TB and that they demonstrate a strong bias toward STB (Figures 1 and 2). Upon PCA, the RNA-seq data from BAP-differentiated cells (H1_BAP_D8_>70_*Yabe* and H1_BAP_D8_<40_*Yabe*) also cluster closely to TB generated from TSCs by Okae et al. (2018) and Io et al. (2021) and to TB from human embryos and placental villi (Figures 4, S4, and S5). Karvas et al. (2020), using a different PCA, have also pointed out the close similarities between BAP-generated cells and the STB differentiated from TSCs by Okae et al. Finally, we observe that multiple clusters of cells/nuclei are shared between the BAP-differentiated cells derived from primed-type PSCs by Khan et al. (2021) and the nTE and more differentiated nCT cells generated from naive PSCs by Io et al. (2021). Together, these data confirm that the BAP protocol generates TB similar, but not identical, to that obtained with other differentiation protocols and that it is distinct from embryonic amnion obtained during pregnancy from 9 weeks to term. Our analyses and conclusions are largely based on using cell-specific enrichment analysis to determine if genes upregulated in BAP-differentiated cells have high expression in certain cells present in the early developing embryo and first-trimester placenta. Direct comparison of gene expression in the early developing amnion with BAP-differentiated cells, and the inclusion of additional early-embryo data, will be necessary to strengthen the conclusions in this work.

One difficulty in defining amnion is that there is presently not a consensus amnion transcriptome nor a robust protein signature for its cell types. Io et al. (2021) compared the genes differentially regulated at day 3 in their protocol

with the transcriptomes of monkey amnion (Ma et al., 2019) and genes upregulated in 9 week placenta compared with 9 week amnion (Roost et al., 2015) and noted some commonalities in terms of gene expression, e.g., upregulation of *GABRP*, *VTCN1*, *CDH10*, *IGFBP2*, *IGFBP5*, *VIM*, *TNC*, and several others, which led them to conclude that their cells (H9_pBAP_D3_*Io*) were amnion and not TB. However, we find that the transcriptome data of H9_pBAP_D3_*Io* also have many features of TB (Figure 2A) and cluster away from those from differentiated amnion (Figure 4A), although at day 3, and particularly at day 2, the Io et al. datasets place relatively closely to the PSC-derived amnion-like cell data of Shao et al. (2017) (H9_amnion_*Shao*). Shao et al. showed high expression *GABRP* and *VTCN1* in their early amnion-sac-like structures derived from PSCs (Shao et al., 2017), while, in fact, some genes expressed in amnion are also well represented in various forms of TB (Table S4), and at least a few, including the aforesaid *GABRP* and *VTCN1*, have been shown by immunohistochemistry performed on placental sections to be expressed as proteins in STB in the first trimester of human pregnancy (Karvas et al., 2020). Further, *GABRP* and *VTCN1* were not considered amnion upregulated when using a tissue-enrichment-based approach compared with cells obtained by using the Okae protocol (Figure 5; Table S5) (Okae et al., 2018). Although we present alternative amnion marker genes, the gene list is based primarily on comparing amnion data generated in one study (Roost et al., 2015) with TB data generated in another (Sheridan et al., 2021). Confirmation of localization of amnion marker genes in the early conceptus by either immunofluorescence or immunohistochemistry will be necessary to confirm our conclusions. It is possible that primed PSCs, while on the way to forming bona fide differentiated TB in response to BMP4-based protocols, may progress through a transcriptional state that possesses amnion-like features. This amnion-like transcriptional state could also be present when TB differentiate *in vivo*, as suggested by Chhabra and Warmflash (2021). This hypothesis will need to be explored further with snRNA-seq time-course studies, which are now ongoing, and with a comparison of each dataset with cell types present in the human embryo.

In summary, this study demonstrates that BAP-treated primed PSCs remain a useful *in vitro* model to investigate the process of TB differentiation and early placental development without necessitating the creation of naïve-type PSCs as the initiating cell source. The accompanying manuscript by Soncin et al. (2022) of *Stem Cell Reports* provides further evidence that primed PSCs can be readily converted to TSCs. The present analyses, which are based on comparisons with data derived from a variety of TB and amnion sources, show that differentiated TB cells can form from primed-type PSCs, although further details of the path taken need to be worked out. The analyses not only provide information about temporal gene-expression changes in PSC-derived TB models but also might give insights into the relationship between epiblast, TB, and amnion at the time the amniotic sac begins to form in the second week of human pregnancy.

EXPERIMENTAL PROCEDURES

RNA-seq analysis

Data were downloaded from the European Nucleotide Archive with enaBrowserTools (v.1.6) (enasequence, 2021). The enaDataGet command was used with the Aspera protocol to download the files directly in fastq format. FastQC (v.0.11.7) (Andrews, 2010) was employed to check the quality of the downloaded files and to obtain the average read length for each library. The fastq files were mapped to a STAR (v.2.5.3a) (Dobin et al., 2013) indexed human reference (GRCh38.p13) (Schneider et al., 2017) that was generated by using the mode genomeGenerate (–runMode genomeGenerate) and with GTF file (–sjdbGTFfile). The read mapping was performed using the mode alignReads (–runMode alignReads) and was optimized for short reads with the options "–outFilterScoreMinOverLread 0.3" and "–outFilterMatchNminOverLread 0.3". Mapping and quantification were done simultaneously using the "–quantMode GeneCounts" option (from GENCODE, GRCh38.p13 - release 37 [Frankish et al., 2021]). The individual count files of each SRA file were merged to generate a single raw count file and filtered to retain only protein-coding genes. The quality-control reports from all preprocessing steps were compiled through the use of MultiQC (Ewels et al., 2016).

The raw count files were imported into R and processed by means of the SVA package (v.3.38.0). We corrected for batch effects or unwanted variation in the data by using the ComBat_seq function of the SVA package (Zhang et al., 2020). A subset (datasets from NCBI-BioProject IDs PRJNA605646, PRJNA294733, and PRJNA414247) of the processed counts were first normalized for library sizes then analyzed to obtain differentially expressed genes by using DESeq2 (v.1.30.1) (Love et al., 2014). Specifically, we retained the genes with counts greater than ten across all conditions and tested for differential expression with the Wald statistical test. The resulting p values were corrected for multiple testing with Benjamini-Hochberg (Benjamini and Hochberg, 1995) to control the false discovery rate (FDR). A total of 8 contrasts were performed (see Data_S1). Differentially expressed (DE) genes were identified after filtering them according to a p value (adjusted) ≤ 0.05 and absolute log2 fold change ≥ 1. Cell enrichment analyses were performed using PlacentaCellEnrich (default settings) (Jain and Tuteja, 2021). We carried out the analyses on the list of DE genes of each comparison with code adapted from the TissueEnrich (v.1.10.1) (Jain and Tuteja, 2019) Bioconductor package. To perform enrichment analyses, we used the scRNA-seq data from first-trimester human placenta (Vento-Tormo et al., 2018), along with custom enrichment datasets (prepared using TissueEnrich; see supplemental experimental procedures). The custom enrichment datasets

were prepared with the data from Xiang et al. (2020) and by Castel et al. (we used the combined Zhou et al. (2019) and Petropoulos et al. (2016) datasets compiled by Castel et al.) (Castel et al., 2020; Petropoulos et al., 2016; Zhou et al., 2019).

The complete count table (batch corrected) was subjected to variance-stabilizing transformation (VST), and clustering was performed with the top 500 variable genes. We performed PCA on the transformed counts using the prcomp() function of the stats library (v.4.0.5). Additional PCA was carried out on differentiated samples to examine the groupings more closely.

Gene expression heatmaps were generated by subsetting the normalized table, filtering the desired genes by using the pheatmap (v.1.0.12) package, and providing the custom annotation for grouping samples.

snRNA- and scRNA-seq analyses

snRNA-seq analysis was performed as described previously (Khan et al., 2021), except we included 4 additional single-cell samples (H9_sc.nTE_D2_*Io*, H9_sc.nTE_D3_*Io*, H9_sc.nCT_D5_*Io*, and H9_sc.nCT_D10_*Io*) (Io et al., 2021). Additional details are in the supplemental experimental procedures.

Identifying amnion markers

For identifying the marker genes, the batch-corrected counts table (prepared previously, see RNA-seq analysis section) was converted into a TPM table by using R. A subset of this table containing only amnion datasets (Roost et al., 2015) and TB cell data (Sheridan et al., 2021) was used as input for teGeneRetrieval function of the TissueEnrich Bioconductor package. Datasets for amnion included seven samples (amnion of 9, 18, and 22 weeks, with two replicates each, and amnion of 16 weeks with one replicate), and 15 samples for TB cells (two replicates each for BT_EVT_*Okae*, BT_SCT_*Okae*, and BT_TSC_*Okae*, and three replicates each for CT_EVT_*Okae*, CT_SCT_*Okae*, and CT_TSC_*Okae*). Genes were defined as amnion markers if they expressed 10-fold or more in amnion datasets, compared with TB cells. The minimum gene-expression cutoff for the gene to be called expressed was set to 1 (expressedGeneThreshold = 1), and the maximum number of tissues in a group to be called group-enriched genes was set to 2 (maxNumberOfTissues = 2).

Data and code availability

All code used is available and documented at https://github.com/Tuteja-Lab/BAPvsTrophoblast_Amnion. All data processed in this manuscript were downloaded from previously deposited studies (Table S1).

SUPPLEMENTAL INFORMATION

Supplemental information can be found online at https://doi.org/10.1016/j.stemcr.2022.04.014.

AUTHOR CONTRIBUTIONS

Conceptualization, T.E., R.M.R., and G.T.; methodology, A.S.S., H.T.H.V., and G.T.; formal analysis, A.S.S. and H.T.H.V.; validation, A.S.S. and H.T.H.V.; data interpretation, A.S.S., H.T.H.V., S.C., T.K., M.A.S., T.E., R.M.R., and G.T.; writing, A.S.S., H.T.H.V., S.C., T.K., M.A.S., T.E., R.M.R., and G.T.; supervision, T.E., R.M.R., and G.T.; funding acquisition, T.E., R.M.R., and G.T.

CONFLICTS OF INTERESTS

The authors declare no competing interests.

ACKNOWLEDGMENTS

This work used HPC equipment at Iowa State University, some of which has been purchased through funding provided by NSF under MRI grant number 1726447. We also acknowledge the Research IT group at Iowa State University (http://researchit.las.iastate.edu) for providing servers and IT support. Research reported in this publication was supported by the Eunice Kennedy Shriver National Institute of Child Health & Human Development of the National Institutes of Health under award numbers R01HD096083 (contact principal investigator [PI]: G.T.), R01HD094937 (contact PI: R.M.R.), and R21A1145071 (contact PI: Danny J. Schust).

Received: August 26, 2021
Revised: March 24, 2022
Accepted: April 19, 2022
Published: May 19, 2022

REFERENCES

Amita, M., Adachi, K., Alexenko, A.P., Sinha, S., Schust, D.J., Schulz, L.C., Roberts, R.M., and Ezashi, T. (2013). Complete and unidirectional conversion of human embryonic stem cells to trophoblast by BMP4. Proc. Natl. Acad. Sci. U S A *110*, E1212–E1221. https://doi.org/10.1073/pnas.1303094110.

Andrews, S. (2010). Babraham bioinformatics - FastQC A quality control tool for high throughput sequence data. https://www.bioinformatics.babraham.ac.uk/projects/fastqc/.

Benjamini, Y., and Hochberg, Y. (1995). Controlling the false discovery rate: a practical and powerful approach to multiple testing. J. R. Stat. Soc. Ser. B Methodol. *57*, 289–300. https://doi.org/10.1111/j.2517-6161.1995.tb02031.x.

Castel, G., Meistermann, D., Bretin, B., Firmin, J., Blin, J., Loubersac, S., Bruneau, A., Chevolleau, S., Kilens, S., Chariau, C., et al. (2020). Induction of human trophoblast stem cells from somatic cells and pluripotent stem cells. Cell Rep. *33*, 108419. https://doi.org/10.1016/j.celrep.2020.108419.

Chhabra, S., and Warmflash, A. (2021). BMP-treated human embryonic stem cells transcriptionally resemble amnion cells in the monkey embryo. Biol. Open *10*, bio058617. https://doi.org/10.1242/bio.058617.

Dobin, A., Davis, C.A., Schlesinger, F., Drenkow, J., Zaleski, C., Jha, S., Batut, P., Chaisson, M., and Gingeras, T.R. (2013). STAR: ultrafast universal RNA-seq aligner. Bioinformatics *29*, 15–21. https://doi.org/10.1093/bioinformatics/bts635.

Dunn, O.J. (1964). Multiple comparisons using rank sums. Technometrics *6*, 241–252. https://doi.org/10.1080/00401706.1964.10490181.

enasequence (2021). enaBrowserTools. GitHub - Enasequence/EnaBrowserTools: a collection of scripts to assist in the retrieval of

data from the ENA browser. https://Github.Com/Enasequence/EnaBrowserTools.

Ewels, P., Magnusson, M., Lundin, S., and Käller, M. (2016). MultiQC: summarize analysis results for multiple tools and samples in a single report. Bioinformatics *32*, 3047–3048. https://doi.org/10.1093/bioinformatics/btw354.

Ezashi, T., Telugu, B.P.V.L., and Roberts, R.M. (2012). Model systems for studying trophoblast differentiation from human pluripotent stem cells. Cell Tissue Res. *349*, 809–824. https://doi.org/10.1007/s00441-012-1371-2.

Frankish, A., Diekhans, M., Jungreis, I., Lagarde, J., Loveland, J.E., Mudge, J.M., Sisu, C., Wright, J.C., Armstrong, J., Barnes, I., et al. (2021). Gencode 2021. Nucleic Acids Res. *49*, D916–D923. https://doi.org/10.1093/nar/gkaa1087.

Gao, X., Usas, A., Lu, A., Tang, Y., Wang, B., Chen, C.-W., Li, H., Tebbets, J.C., Cummins, J.H., and Huard, J. (2013). BMP2 is superior to BMP4 for promoting human muscle-derived stem cell-mediated bone regeneration in a critical-sized calvarial defect model. Cell Transpl. *22*, 2393–2408. https://doi.org/10.3727/096368912x658854.

Guo, G., Stirparo, G.G., Strawbridge, S.E., Spindlow, D., Yang, J., Clarke, J., Dattani, A., Yanagida, A., Li, M.A., Myers, S., et al. (2021). Human naive epiblast cells possess unrestricted lineage potential. Cell Stem Cell *28*, 1040–1056.e6. https://doi.org/10.1016/j.stem.2021.02.025.

Horii, M., Li, Y., Wakeland, A.K., Pizzo, D.P., Nelson, K.K., Sabatini, K., Laurent, L.C., Liu, Y., and Parast, M.M. (2016). Human pluripotent stem cells as a model of trophoblast differentiation in both normal development and disease. Proc. Natl. Acad. Sci. U S A. *113*, E3882–E3891. https://doi.org/10.1073/pnas.1604747113.

Horii, M., Bui, T., Touma, O., Cho, H.Y., and Parast, M.M. (2019). An improved two-step protocol for trophoblast differentiation of human pluripotent stem cells. Curr. Protoc. Stem Cell Biol. *50*, e96. https://doi.org/10.1002/cpsc.96.

Horii, M., Touma, O., Bui, T., and Parast, M.M. (2020). Modeling human trophoblast, the placental epithelium at the maternal fetal interface. Reproduction *160*, R1–R11. https://doi.org/10.1530/rep-19-0428.

Io, S., Kabata, M., Iemura, Y., Semi, K., Morone, N., Minagawa, A., Wang, B., Okamoto, I., Nakamura, T., Kojima, Y., et al. (2021). Capturing human trophoblast development with naive pluripotent stem cells in vitro. Cell Stem Cell *28*, 1023–1039.e13. https://doi.org/10.1016/j.stem.2021.03.013.

Jain, A., and Tuteja, G. (2019). TissueEnrich: tissue-specific gene enrichment analysis. Bioinformatics *35*, 1966–1967. https://doi.org/10.1093/bioinformatics/bty890.

Jain, A., and Tuteja, G. (2021). PlacentaCellEnrich: a tool to characterize gene sets using placenta cell-specific gene enrichment analysis. Placenta *103*, 164–171. https://doi.org/10.1016/j.placenta.2020.10.029.

James, D., Levine, A.J., Besser, D., and Hemmati-Brivanlou, A. (2005). TGFβ/activin/nodal signaling is necessary for the maintenance of pluripotency in human embryonic stem cells. Development *132*, 1273–1282. https://doi.org/10.1242/dev.01706.

Karvas, R.M., McInturf, S., Zhou, J., Ezashi, T., Schust, D.J., Roberts, R.M., and Schulz, L.C. (2020). Use of a human embryonic stem cell model to discover GABRP, WFDC2, VTCN1 and ACTC1 as markers of early first trimester human trophoblast. Mol. Hum. Reprod. *26*, 425–440. https://doi.org/10.1093/molehr/gaaa029.

Khan, T., Seetharam, A.S., Zhou, J., Bivens, N.J., Schust, D.J., Ezashi, T., Tuteja, G., and Roberts, R.M. (2021). Single nucleus RNA sequence (snRNAseq) analysis of the spectrum of trophoblast lineages generated from human pluripotent stem cells in vitro. Front. Cell Dev. Biol. *9*, 695248. https://doi.org/10.3389/fcell.2021.695248.

Krendl, C., Shaposhnikov, D., Rishko, V., Ori, C., Ziegenhain, C., Sass, S., Simon, L., Müller, N.S., Straub, T., Brooks, K.E., et al. (2017). GATA2/3-TFAP2A/C transcription factor network couples human pluripotent stem cell differentiation to trophectoderm with repression of pluripotency. Proc. Natl. Acad. Sci. U S A *114*, E9579–E9588. https://doi.org/10.1073/pnas.1708341114.

Kruskal, W.H., and Wallis, W.A. (1952). Use of ranks in one-criterion variance analysis. J. Am. Stat. Assoc. *47*, 583–621. https://doi.org/10.1080/01621459.1952.10483441.

Love, M.I., Huber, W., and Anders, S. (2014). Moderated estimation of fold change and dispersion for RNA-seq data with DESeq2. Genome Biol. *15*, 550. https://doi.org/10.1186/s13059-014-0550-8.

Ma, H., Zhai, J., Wan, H., Jiang, X., Wang, X., Wang, L., Xiang, Y., He, X., Zhao, Z.-A., Zhao, B., et al. (2019). In vitro culture of cynomolgus monkey embryos beyond early gastrulation. Science *366*, eaax7890. https://doi.org/10.1126/science.aax7890.

Marchand, M., Horcajadas, J.A., Esteban, F.J., McElroy, S.L., Fisher, S.J., and Giudice, L.C. (2011). Transcriptomic signature of trophoblast differentiation in a human embryonic stem cell Model1. Biol. Reprod. *84*, 1258–1271. https://doi.org/10.1095/biolreprod.110.086413.

Okae, H., Toh, H., Sato, T., Hiura, H., Takahashi, S., Shirane, K., Kabayama, Y., Suyama, M., Sasaki, H., and Arima, T. (2018). Derivation of human trophoblast stem cells. Cell Stem Cell *22*, 50–63.e6. https://doi.org/10.1016/j.stem.2017.11.004.

Petropoulos, S., Edsgärd, D., Reinius, B., Deng, Q., Panula, S.P., Codeluppi, S., Plaza Reyes, A., Linnarsson, S., Sandberg, R., and Lanner, F. (2016). Single-cell RNA-seq reveals lineage and X chromosome dynamics in human preimplantation embryos. Cell *165*, 1012–1026. https://doi.org/10.1016/j.cell.2016.03.023.

Roberts, R.M., Ezashi, T., Sheridan, M.A., and Yang, Y. (2018). Specification of trophoblast from embryonic stem cells exposed to BMP4. Biol. Reprod. *99*, 212–224. https://doi.org/10.1093/biolre/ioy070.

Roost, M.S., van Iperen, L., Ariyurek, Y., Buermans, H.P., Arindrarto, W., Devalla, H.D., Passier, R., Mummery, C.L., Carlotti, F., de Koning, E.J.P., et al. (2015). KeyGenes, a tool to probe tissue differentiation using a human fetal transcriptional Atlas. Stem Cell Rep. *4*, 1112–1124. https://doi.org/10.1016/j.stemcr.2015.05.002.

Schneider, V.A., Graves-Lindsay, T., Howe, K., Bouk, N., Chen, H.-C., Kitts, P.A., Murphy, T.D., Pruitt, K.D., Thibaud-Nissen, F., Albracht, D., et al. (2017). Evaluation of GRCh38 and de novo haploid genome assemblies demonstrates the enduring quality of

the reference assembly. Genome Res. *27*, 849–864. https://doi.org/10.1101/gr.213611.116.

Schulz, L.C., Ezashi, T., Das, P., Westfall, S.D., Livingston, K.A., and Roberts, R.M. (2008). Human embryonic stem cells as models for trophoblast differentiation. Placenta *29 Suppl A*, S10–S16. https://doi.org/10.1016/j.placenta.2007.10.009.

Shao, Y., Taniguchi, K., Gurdziel, K., Townshend, R.F., Xue, X., Yong, K.M.A., Sang, J., Spence, J.R., Gumucio, D.L., and Fu, J. (2017). Self-organized amniogenesis by human pluripotent stem cells in a biomimetic implantation-like niche. Nat. Mater. *16*, 419–425. https://doi.org/10.1038/nmat4829.

Sheridan, M.A., Zhao, X., Fernando, R.C., Gardner, L., Perez-Garcia, V., Li, Q., Marsh, S.G.E., Hamilton, R., Moffett, A., and Turco, M.Y. (2021). Characterization of primary models of human trophoblast. Development *148*, dev199749. https://doi.org/10.1242/dev.199749.

Shu, B., Zhang, M., Xie, R., Wang, M., Jin, H., Hou, W., Tang, D., Harris, S.E., Mishina, Y., O'Keefe, R.J., et al. (2011). BMP2, but not BMP4, is crucial for chondrocyte proliferation and maturation during endochondral bone development. J. Cell Sci. *124*, 3428–3440. https://doi.org/10.1242/jcs.083659.

Soncin, F., Morey, R., Bui, T., Requena, D.F., Cheung, V.C., Kallol, S., Kittle, R., Jackson, M.G., Farah, O., Dumdie, J., et al. (2022). Derivation of functional trophoblast stem cells from primed human pluripotent stem cells. Stem Cell Rep. *17*. https://doi.org/10.1016/j.stemcr.2022.04.013.

Suzuki, M., Maekawa, R., Patterson, N.E., Reynolds, D.M., Calder, B.R., Reznik, S.E., Heo, H.J., Einstein, F.H., and Greally, J.M. (2016). Amnion as a surrogate tissue reporter of the effects of maternal preeclampsia on the fetus. Clin. Epigenetics *8*, 67. https://doi.org/10.1186/s13148-016-0234-1.

Telugu, B.P., Adachi, K., Schlitt, J.M., Ezashi, T., Schust, D.J., Roberts, R.M., and Schulz, L.C. (2013). Comparison of extravillous trophoblast cells derived from human embryonic stem cells and from first trimester human placentas. Placenta *34*, 536–543. https://doi.org/10.1016/j.placenta.2013.03.016.

Tsang, J.C.H., Vong, J.S.L., Ji, L., Poon, L.C.Y., Jiang, P., Lui, K.O., Ni, Y.-B., To, K.F., Cheng, Y.K.Y., Chiu, R.W.K., and Lo, Y.M.D. (2017). Integrative single-cell and cell-free plasma RNA transcriptomics elucidates placental cellular dynamics. PNAS *114*, E7786–E7795. https://doi.org/10.1073/pnas.1710470114.

Uhlén, M., Fagerberg, L., Hallström, B.M., Lindskog, C., Oksvold, P., Mardinoglu, A., Sivertsson, Å., Kampf, C., Sjöstedt, E., Asplund, A., et al. (2015). Proteomics. Tissue-based map of the human proteome. Science *347*, 1260419. https://doi.org/10.1126/science.1260419.

Vento-Tormo, R., Efremova, M., Botting, R.A., Turco, M.Y., Vento-Tormo, M., Meyer, K.B., Park, J.-E., Stephenson, E., Polański, K., Goncalves, A., et al. (2018). Single-cell reconstruction of the early maternal-fetal interface in humans. Nature *563*, 347–353. https://doi.org/10.1038/s41586-018-0698-6.

Xiang, L., Yin, Y., Zheng, Y., Ma, Y., Li, Y., Zhao, Z., Guo, J., Ai, Z., Niu, Y., Duan, K., et al. (2020). A developmental landscape of 3D-cultured human pre-gastrulation embryos. Nature *577*, 537–542. https://doi.org/10.1038/s41586-019-1875-y.

Xu, R.-H., Chen, X., Li, D.S., Li, R., Addicks, G.C., Glennon, C., Zwaka, T.P., and Thomson, J.A. (2002). BMP4 initiates human embryonic stem cell differentiation to trophoblast. Nat. Biotechnol. *20*, 1261–1264. https://doi.org/10.1038/nbt761.

Yabe, S., Alexenko, A.P., Amita, M., Yang, Y., Schust, D.J., Sadovsky, Y., Ezashi, T., and Roberts, R.M. (2016). Comparison of syncytiotrophoblast generated from human embryonic stem cells and from term placentas. Proc. Natl. Acad. Sci. U S A *113*, E2598–E2607. https://doi.org/10.1073/pnas.1601630113.

Yang, Y., Adachi, K., Sheridan, M.A., Alexenko, A.P., Schust, D.J., Schulz, L.C., Ezashi, T., and Roberts, R.M. (2015). Heightened potency of human pluripotent stem cell lines created by transient BMP4 exposure. Proc. Natl. Acad. Sci. U S A *112*, E2337–E2346. https://doi.org/10.1073/pnas.1504778112.

Yang, L., Liu, S., and Wang, Y. (2019). Role of bone morphogenetic protein-2/4 in astrocyte activation in neuropathic pain. Mol. Pain *15*. 174480691989210. https://doi.org/10.1177/1744806919892100.

Zhang, Y., Parmigiani, G., and Johnson, W.E. (2020). ComBat-seq: batch effect adjustment for RNA-seq count data. NAR Genom. Bioinform. *2*, lqaa078. https://doi.org/10.1093/nargab/lqaa078.

Zhou, F., Wang, R., Yuan, P., Ren, Y., Mao, Y., Li, R., Lian, Y., Li, J., Wen, L., Yan, L., et al. (2019). Reconstituting the transcriptome and DNA methylome landscapes of human implantation. Nature *572*, 660–664. https://doi.org/10.1038/s41586-019-1500-0.

Zhou, J., West, R.C., Ehlers, E.L., Ezashi, T., Schulz, L.C., Roberts, R.M., Yuan, Y., and Schust, D.J. (2021). Modeling human peri-implantation placental development and function. Biol. Reprod. *105*, 40–51. https://doi.org/10.1093/biolre/ioab080.